Chemical Engineering Journal 497 (2024) 154579

Contents lists available at ScienceDirect

Chemical Engineering Journal

journal homepage: www.elsevier.com/locate/cej

Unravelling the complexity of hemicellulose pyrolysis: Quantitative and detailed product speciation for xylan and glucomannan in TGA and fixed bed reactor

Veronica Piazza [a], Roberto Batista da Silva Junior [a,1], Alessio Frassoldati [b], Luca Lietti [a], Chiara Gambaro [c], Kishore Rajendran [d], De Chen [d], Tiziano Faravelli [b], Alessandra Beretta [a,*]

[a] Laboratory of Catalysis and Catalytic Processes, Dipartimento di Energia, Politecnico di Milano, 20156 Milano, Italy
[b] CRECK Modeling group, Dipartimento di Chimica, Materiali e Ingegneria Chimica, Politecnico di Milano, 20133 Milano, Italy
[c] ENI Novara Laboratories (CENTR), 28100 Novara, Italy
[d] Catalysis group, Department of Chemical Engineering, Norwegian University of Science and Technology, 7491 Trondheim, Norway

ARTICLE INFO

Keywords:
Pyrolysis
Hemicellulose
Xylan
Glucomannan
TGA
Fixed bed
Kinetic modelling

ABSTRACT

For the first time, the complete characterization of the pyrolysis of key biomass components – xylan (representative of pentose-based hardwood hemicellulose) and glucomannan (representative of hexose-based softwood hemicellulose) – is herein obtained by applying a novel methodology based on TGA (thermogravimetric analysis), previously developed for cellulose. Data on devolatilization rates, onset temperatures and detailed quantification of the mass yield of ~ 50 products in the gas, liquid, solid phase were achieved simultaneously, with closure of mass balance, thus providing unique kinetic information. Pyrolysis tests were also carried out in a fixed bed reactor to explore larger scales and validate the TGA-based approach. At both scales, combinations of different analytical techniques (online MS, offline GC-FID/MS, Karl Fischer titration) and sampling protocols (cold condenser, sorbent traps, vapour syringes, gas bags) were tuned to achieve closure of mass balances and rigorous product speciation.

While the pyrolysis of cellulose – chosen as reference system – maximized the bio-oil production (mostly levoglucosan), the pyrolysis of xylan resulted into an even distribution among solid, liquid and gas phases, with condensable oxygenates spanning homogeneously in the C_1-C_9 range. Interestingly, glucomannan showed an intermediate behaviour between cellulose and xylan, mirroring its intermediate chemical structure. Raman and oxidation analyses on the collected char samples showed that the solid residuals from hemicelluloses were less ordered and richer in ashes than those from cellulose.

The predictions of recent lumped kinetic models were used to benchmark the new datasets against the prior art on hemicellulose pyrolysis; the richness and comprehensiveness of the new information clearly emerge and pave the pathway to the de-bottlenecking of kinetic modelling.

1. Introduction

The valorisation of biomass resources is emerging as a pivotal area of research and development. In this context, thermochemical processes like gasification, pyrolysis and liquefaction, gain strategic importance due to their capacity to convert a complex feedstock as lignocellulosic biomass into valuable bio-fuels, bio-chemicals, energy carriers and other high-value products [1–7]. This approach aligns with the principles of circular economy, since enables the valorisation of wastes from agricultural and forest industries [8–10]. Besides, biomass stands out as a valuable renewable energy source to pursue the energy transition: for instance, advanced biofuels will play a key role to meet the 29 % share of

Abbreviations: Aro, aromatics; Cy, cyclic oxygenates (non-furanic, non-aromatic); Fur, furanic species; Ket, aliphatic ketones and aldehydes; Lin, aliphatic alcohols, carboxylic acids, anhydrides, ethers; Sug, anhydrosugars, monosaccharides; TG curve, thermogravimetric curve; DTG curve, differential thermogravimetric curve; TGA, thermogravimetric analysis; TPO, temperature programmed oxidation.

* Corresponding author.
E-mail address: alessandra.beretta@polimi.it (A. Beretta).
[1] SENAI CIMATEC, Av. Orlando Gomes, 1845 – Piatã, 41650-010 Salvador - BA, Brazil (Present address).

https://doi.org/10.1016/j.cej.2024.154579
Received 29 February 2024; Received in revised form 30 July 2024; Accepted 4 August 2024
Available online 5 August 2024

renewable energy sources within the transportation sector outlined for 2030 in RED III (Renewable Energy Directive) [11].

The process of pyrolysis is characterised by the thermal devolatilization of lignocellulosic biomass in an inert atmosphere, resulting in the production of biochar, bio-oil and a gas stream. Moreover, the pyrolysis stage, seen as devolatilization stage, constitutes the first phase of biomass gasification and combustion; therefore, the study of pyrolysis is of fundamental importance for the entire range of thermochemical processes. Nevertheless, there is a lack of fundamental knowledge on biomass pyrolysis chemistry, which is restraining the development of technologies for all thermal processes. There is indeed an awareness of the intrinsic complexities of pyrolysis, which mostly originate from the multifaceted chemical structure of the feedstock [12].

Lignocellulosic materials are a very attractive class of biomasses. They are heterogenous polymeric materials, composed of cellulose, hemicellulose and lignin as main constituents, alongside traces of pectins, proteins and minerals [13,14]. Lignin is a crosslinked macromolecular species based on phenylpropanoid monomers [15], while cellulose and hemicellulose are polysaccharides. In particular, cellulose is a linear homogenous polymer composed of β-1,4-linked D-glucose units that is well structured and contains crystalline regions. In contrast, hemicellulose is a mixture of amorphous and partially branched polysaccharides, that are characterized by being easily devolatilized or hydrolysed in dilute acid or base, but that differ significantly in terms of structure and physicochemical properties [14]. A clear definition of hemicellulose polysaccharides is reported by Zhou et al. [14], where five groups are identified: xylans, mannans, xyloglucans, β-glucans and galactans. These are homogeneous and heterogeneous polysaccharides that contain both pentose – xylose, arabinose – and hexose – glucose, mannose, galactose – monosaccharides. Hardwood hemicellulose is mainly composed of xylan (15–30 % content in dry biomass), but also glucomannan (1–5 %). Glucomannan is instead the major component in softwood (10–15 %), where arabinoxylans (7–10 %), galacto- and *gluco*-mannans (5–8 %) are also present. Herbaceous biomass is formed by arabinoxylans, together with minor contents of mannans, xyloglucans and glucans [16–18].

This intricate chemical structure of the bio-feedstock is reflected into an extreme complexity of the pyrolysis product slate, giving rise to a wide spectrum of oxygenates and drastically impacting the physical–chemical properties of the bio-oil. This multi-component feature makes the formalization of kinetic schemes challenging. To address this challenge, there is a strong need for studying biomass pyrolysis with a fundamental approach, aiming to the obtainment of accurate kinetic data on devolatilization, the methodical screening of different biomass types, the development of versatile mathematical models for kinetics and reactor simulation [19,20].

Semi-detailed lumped kinetic schemes represent a possible approach to address the kinetic modelling of biomass pyrolysis: they are semi-empirical models that address biomass devolatilization with lumped stoichiometries and lumped species, with the goal of describing both devolatilization kinetics and product distribution. These schemes represent a compromise between detailed mechanistic models which try to reproduce the mechanism of pyrolysis, and global models, that uniquely focus on overall yields of gas, tar and char fractions, and apparent activation energies [19,20]. A lumped scheme of biomass pyrolysis was initially developed by some of the authors [21–25], and has been subsequently refined and improved by Dussan et al. [16] and Debiagi et al. [26]. In this modelling approach, biomass is characterized in terms of macro-constituents: cellulose, hemicellulose and lignin. The global behaviour of real biomasses is obtained as a linear combination of the contributions of the single constituents. Therefore, the accuracy of these models mirrors the accuracy of the experimental data on cellulose, hemicellulose and lignin that were utilized for their tuning.

The study of hemicellulose pyrolysis kinetics is an open research challenge. State-of-the-art lumped kinetic schemes, which have been reviewed by Dussan et al. [16], are able to well predict devolatilization trends. However, the description of product distribution in the latest model revisions [16,21,26] remains critical, since the tuning and validation of lumped models is limited by the complex harvesting of experimental datasets, which are partial and fragmentary, in particular in the case of hemicelluloses. In fact:

- for devolatilization curves, several studies in thermogravimetric analysers (TGAs) were employed to describe the behaviour of different hemicellulosic polysaccharides [27–35];
- for light pyrolysis products as gases and H_2O, experimental data were mainly obtained from TGA-setups equipped with online analytical instruments (e.g. FTIR, MS) [29–34]. These setups enable the tracking of light gases and H_2O evolution, although only qualitative trends are mostly reported. Selected oxygenates are only occasionally monitored;
- for condensable oxygenates, experimental data from micro-pyrolyzers [32,34], fixed bed reactors [28,31] and fluidized bed reactors [29,36] were utilized. However, these configurations do not provide information on devolatilization kinetics and may be affected by transfer limitations and onset of undesired secondary reactions, that can compromise the kinetic analysis. Moreover, analogies to cellulose were also taken into account, due to the lack of specific data.

Advancement in the fundamental understanding of hemicellulose thermal degradation is now essential to improve the accuracy of kinetic models, as also stated by Dussan and co-authors [16]. For this reason, the development of an experimental protocol able to provide accurate and complete kinetic information, with identification of the entire product slate and the closure of mass balance, is imperative for developing and validating lumped kinetic schemes. In this context, the authors have presented in a previous study [37] a novel TGA-based methodology that for the first time integrates the acquisition of kinetic data on biomass devolatilization with a rigorous quantitative characterization of the entire product slate. Besides, the TG setup is extremely suitable for modelling purposes, since it can be simply described with a zero-dimensional reactor and directly provides onset temperatures. As proof of the efficacy of this methodology, experimental data of cellulose pyrolysis were then successfully used to develop a refined kinetic scheme, with new reactions and lumped products [38]. This demonstrated the potential of this methodology to be extended to the kinetic study of other biomass components, ensuring the generation of high-quality, accurate data of significant value.

The main goal of the present work is to provide a complete and quantitative experimental dataset on two bio-constituents of key importance: xylan (representative of pentose-based hardwood hemicellulose) and glucomannan (representative of hexose-based softwood hemicellulose). This dataset is intended to close the lack of systematic and comprehensive kinetic characterization of the reacting system, along the lines of the best standards in chemical reaction engineering; at the scope, the previous experience of the authors in the kinetic study of complex reaction systems has been valorised [21,22,31,39–43]. To this purpose, hemicellulose pyrolysis experiments were performed with a TGA-based methodology previously developed on cellulose, to collect intrinsic rate measurements combined with detailed and quantitative speciation. Pyrolysis experiments were also carried out in a fixed bed reactor to explore a more representative scale and validate the TGA-based approach.

Experimental results were compared with the predictions of state-of-the-art lumped models [16,26], aiming to highlight the game-changing nature of the new experimental data. At the best of our knowledge, they provide unique information, not available in the literature so far.

2. Material and methods

2.1. Materials

In this study, pyrolysis experiments were carried out using commercial powders. Beechwood-derived xylan (Megazyme International) and Konjac-derived glucomannan (low viscosity, Megazyme International) were chosen to respectively represent the pentose-based and the hexose-based fractions of hemicellulose. The xylan was characterized by a xylose:glucuronic acid ratio of 7.1 and a 7.8 % content of other sugar compounds, whereas a mannose:glucose ratio of 60:40 was declared for glucomannan. Microcrystalline cellulose from Sigma Aldrich, with average particle size of 20 μm, was selected as cellulose representative and as a benchmark to discuss results from hemicelluloses. Table 1 reports further details on sugar composition and molecular structure of these biomass constituents.

The samples were used without pre-treatment in the case of TGA testing, while for the experiments in fixed bed reactor the powders were pressed, ground and sieved to achieve a particle size within the range of 420–640 μm. This adjustment was made to fit the wire used to hold biomass during testing (described in section 2.3).

2.2. TGA-based methodology for pyrolysis tests

Pyrolysis experiments were carried out with a novel TGA-based methodology specifically developed to achieve a complete characterization of the product slate. Fig. 1 displays a schematization of this methodology, presented and described in [37].

Briefly, biomass samples of 7–20 mg were placed inside a thermogravimetric analyser (TGA, Hitachi STA7300 TG-DTA) and heated up at controlled heating rates ranging from 3 °C/min to 100 °C/min. During the tests, a continuous flow of He was employed to convey the pyrolysis products released in the vapour phase outside the TGA chamber. The He flowrate varied in the range of 75–285 ml(NTP)/min according to the fractions of products of interest, as largely described in [37]. Mass loss curves (TG curves) and derivative mass loss curves (DTG) were tracked during the experiments.

Gases (CO, CO_2, CH_4, C_2H_x) and H_2O were analysed online with a quadrupole mass spectrometer (HPR-20 EGA, Hidden Analytical) with SEM (Secondary Electron Multiplier) detector, connected to TGA-chamber with a quartz inert capillary line (heated at 250 °C). The real-time monitoring of gas and H_2O production during pyrolysis tests enabled the direct association of their production peaks with TG curves. An uncertainty of ± 3.0 % was estimated for CO_x yield, ± 3.6 % for H_2O yield and ± 0.3 % for the yield of other gas species.

Identification and quantification of the condensable pyrolysis products (i.e. oxygenated compounds in the range of C_1-C_9) were performed using an offline GC-FID/MS instrument (Agilent 6890, 5973 MSD) equipped with a HP-5MS capillary column (30 m x 250 μm x 0.25 μm). Analyses in GC–MS were used to identify the species in the mixture using a National Institute of Standards and Technology (NIST) mass spectral library, while the quantification relied on GC-FID chromatograms.

A dual sampling protocol was designed for the collection of condensable pyrolysis products for offline GC analysis. On one side, vapours at the TGA chamber outlet were sampled using a 2.5 mL gas syringe at the point of maximum devolatilization rate. On the other side, Orbo-609 traps (Supelco) were connected at the TGA chamber outlet to capture condensable pyrolysis products, usually the heaviest ones. At the end of the experiments, the traps were washed using an acetone-based solution containing a known amount of 1-Fluoronaphthalene, used as internal standard for quantitative analysis. The obtained liquid mixture was injected into the GC–MS/FID for species identification and quantification. Further notes about the experimental protocol are reported in [37] and in Supplementary Material (section S.1).

The integral mass yield of each pyrolysis product was determined, as in Eq. (1).

$$Y_i = \frac{m_i}{m_{bio,0}} \times 100\ [\%] \tag{1}$$

where $m_{bio,0}$ and m_i represent respectively the initial mass of biomass and the total mass of the single species or the class of compounds i produced at the end of the pyrolysis experiment.

The combination of online gas measurements with MS, off-line analysis of the vapours (at the point of maximum evolution) and integral analysis of condensable species inside Orbo traps enabled to check mass balances and to assess the goodness of the experiment.

2.3. Fixed bed reactor for pyrolysis tests

Pyrolysis experiments in fixed bed configuration were performed in a vertical laboratory-scale reactor. A tubular stainless-steel reactor (I.D. 22 mm) was heated externally by an electrical oven and the temperature was controlled using a K-thermocouple in contact with its external wall. To enhance heat transfer, the reactor was inserted inside a copper enclosure. During the experiment, a N_2 flow of 166 ml(NTP)/min was flown, regulated by a Bronkhorst mass flow controller. The biomass sample (0.5 g of cellulose, xylan or glucomannan powders) was placed in a separated cold zone above the reactor under Ar flow. The powders

Table 1
Biomass tested in this study.

Biomass	Sugar composition	Molecular structure
Xylan	Xylose: 80.8 % Glucuronic acid: 11.4 % Other sugars: 7.8 %	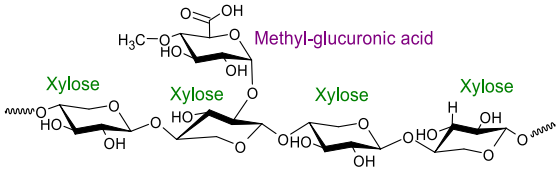
Glucomannan	Mannose: 60 % Glucose: 40 %	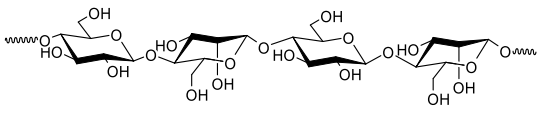
Cellulose	Glucose: 100 %	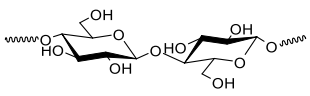

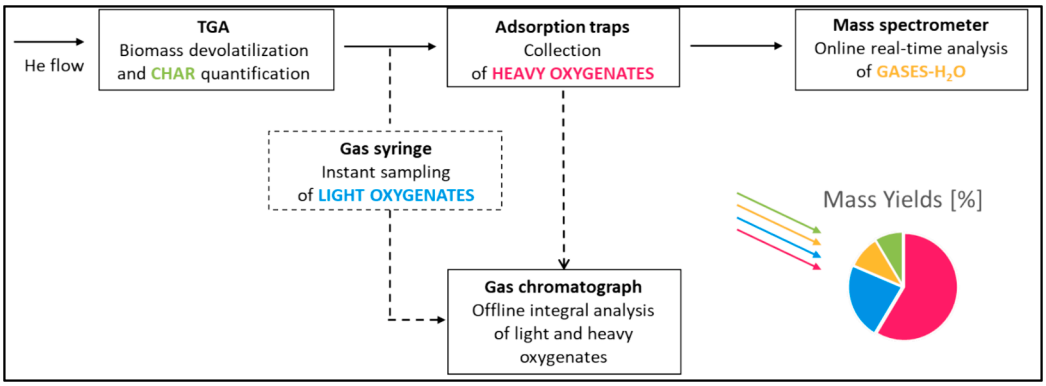

Fig.1. TGA-based methodology for biomass pyrolysis tests with comprehensive product speciation [37].

were placed inside a stainless-steel wire (I.D. 15 mm) between two beds of quartz wool. When the reactor reached the desired temperature (500 °C or 550 °C) and after 1 h stabilization hold, the wire containing the biomass was dropped inside the reactor and stopped in the central area of the furnace.

The volatiles evolving from the reactor during the pyrolysis phase were passed inside a glass condenser cooled down to −17 °C using a water-ethylene glycol mixture, where condensable species were entrapped. The condenser was placed just below the reactor and connected with a transfer line heated at 250 °C. Gas products were collected in a gas bag during the entire duration of the experiment. Each test lasted 8.5 min, after which both the gas bag and the condenser were disconnected. A continuous N_2 flow of 10 ml(NTP)/min was flown inside the reactor during the cooling phase to prevent char combustion.

The composition of the gaseous mixture stored in the gas bag was analysed in an Agilent gas chromatograph, equipped with Molesieve 5A and Porapak Q columns, and two detectors (TCD, FID). The integral mass yield of each gas product (CO, CO_2, CH_4, light hydrocarbons) was evaluated using N_2 as internal standard.

The condenser was washed with tetrahydrofuran (THF) to extract the bio-oil collected during the experiment and a known amount of dichloromethane (DCM) was added as internal standard for GC analyses. Calibration factors were calculated by analysing THF solutions with known amount of DCM and a large number of analytical standards, representing the major detected products. The composition of the mixture was analysed using a GC–MS (Agilent 7820A, 5977E MSD) instrument for species identification and a GC-FID (Agilent 7820A) for species quantification. A custom-made polar capillary column was used. During the analysis, GC oven was initially set at 40 °C for 20 min and then heated up to 80 °C at 1 °C/min, and then at 110 °C, 150 °C, 160 °C and 290 °C at a rate of 2 °C/min, with a hold time of 10 min at each temperature. The column was operated with a constant He flowrate of 3 ml/min and with a H_2/air ratio of (35 mL/min)/(350 mL/min) in FID detector.

The water content of the bio-oil was obtained via volumetric Karl-Fischer titration (V20S Compact Volumetric Titrator, Mettler Toledo). An uncertainty of ± 5 % on mass yield was estimated.

By combining these composition analyses with the weighing protocol involving pre- and post- experiment measurements, the integral mass yield of the bio-oil as well as of each individual condensable product were determined.

Additionally, the amount of solid residual was quantified by measuring the weight of the wire before and after the experiment.

2.4. Characterization of char

The char samples collected from experiments in the fixed bed reactor were characterized.

Raman spectra were recorded at room temperature on a Horiba Jobin Yvon LabRAM HR800 UV spectrometer, using a laser emitting at 633 nm and a 50x objective.

Temperature Programmed Oxidation (TPO) measurements were performed in a Netzsch thermogravimetric analyser (STA 449C), where the mass change was monitored during the tests. Char samples, weighing between 9 mg and 13 mg, were heated to 900 °C using a temperature ramp of 5 °C/min, while flowing a gas stream composed of air (60 ml (NTP)/min) and Ar (20 ml(NTP)/min).

2.5. Lumped kinetic models

The two lumped kinetic schemes proposed by Debiagi et al. [26] and by Dussan et al. [16] were employed for the simulations of xylan and glucomannan pyrolysis. For cellulose, only the model of Debiagi et al. [26] was used, as Dussan and co-workers [16] have focused exclusively on hemicellulose. In this work, experimental data are compared with model predictions to underscore the potential benefits of a complete dataset for models upgrading.

The kinetic scheme, stoichiometries and kinetic parameters for hemicellulose pyrolysis are reported in Tables S1 and S2 in the Supplementary Material (section S.2). The cellulose scheme, which served as reference for hemicellulose analysis, was described in [37].

TGA experiments were simulated in OpenSMOKE++ [44], where the lumped mechanism was integrated into a zero-dimensional reactor model. For each simulation, the initial mass of biomass, the inert flowrate and the temperature program were provided as input parameters, and set equal to those used experimentally.

3. Results and discussion

3.1. Thermogravimetric analysis

The devolatilization of glucomannan and xylan were investigated through TGA experiments at different heating rate (3–20-100 °C/min) and the results were compared with analogous experiments carried out with cellulose. Fig. 2 presents the TG and DTG curves (panels A-C-D and B-D-F, respectively), that were refined to the dry weight of each biomass sample, thus eliminating the contribution of moisture release observed below 150 °C. This accounted for approximately 3 % of the initial weight for cellulose, 6 % for glucomannan and 10 % for xylan.

As discussed in [37], cellulose underwent a single-step devolatilization over a narrow temperature range, with a simple TG curve with a distinct and unique drop. The maximum of the DTG peak shifts to higher temperatures with increasing the heating rate, as expected (Fig. 2B, D and F).

Both xylan and glucomannan showed a lower thermal stability compared to cellulose, and underwent decomposition at lower temperatures, consistently with prior literature [28,45–49]. This different behaviour is attributed to the well-organized and partially crystalline

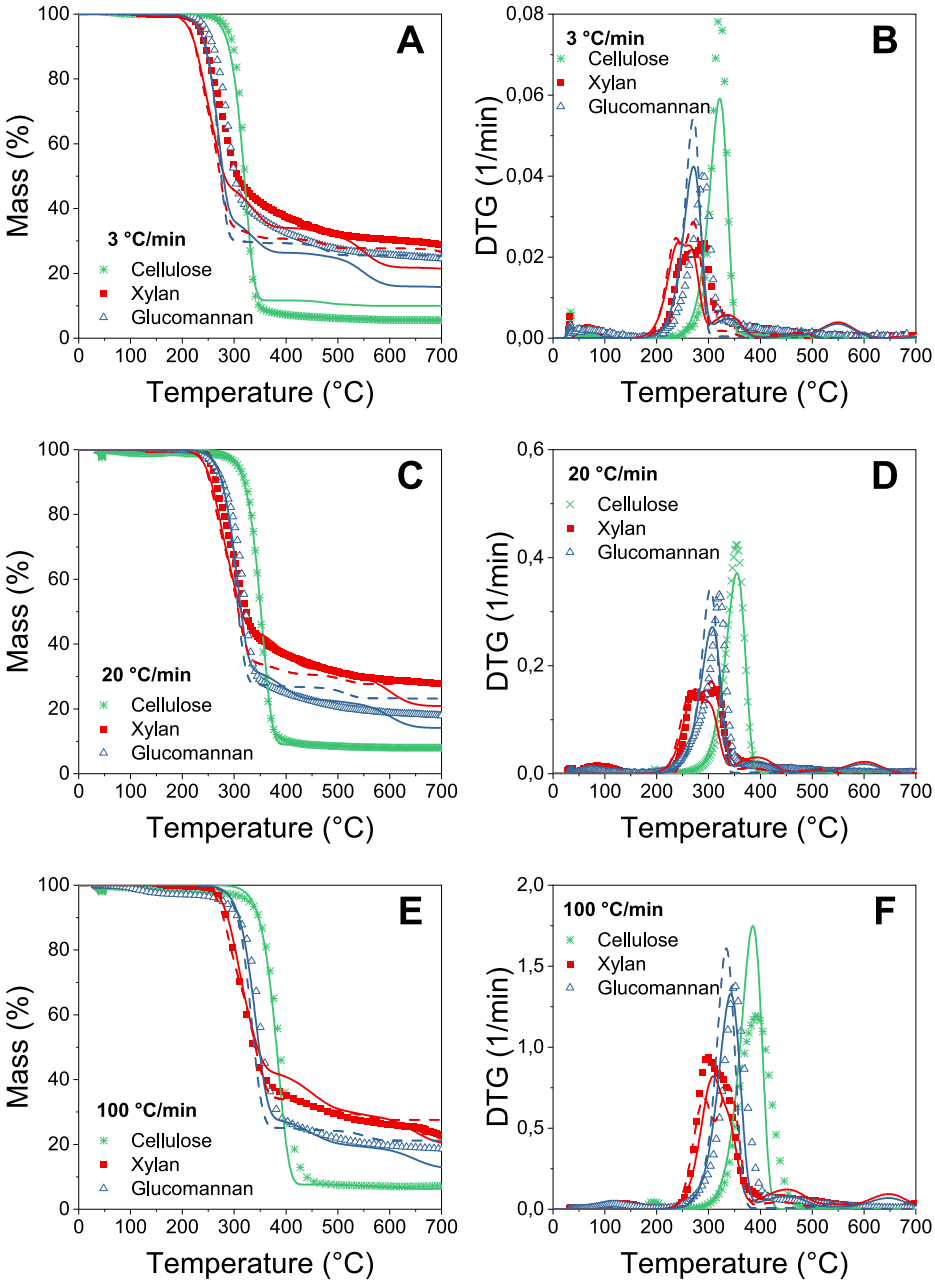

Fig.2. TG and DTG curves of cellulose, xylan and glucomannan at varying heating rate: 3 °C/min (A-B), 20 °C/min (C-D) and 100 °C/min (E-F). Scatters = experimental measurements; solid lines = predictions of the model by Debiagi et al. [26]; dashed lines = predictions of the model by Dussan et al. [16].

structure of cellulose polymer, composed of unbranched chains of D-glucose units. This ordered molecular arrangement enhances the thermal stability and leads to a clearly defined devolatilization step. On the other hand, the amorphous and partially branched structure of hemicellulose polymer results in lower devolatilization temperatures. Moreover, unlike cellulose, hemicellulose TG curves reveal a multi-step decomposition process across a broader temperature window. This multi-faceted behaviour mirrors the inherent diversity of hemicellulosic polymers, both in terms of their structure (single-chain backbones with branches that may undergo partial or complete devolatilization at distinct stages) and their chemical composition, with glucomannan composed of two monomers and xylan containing the glucuronic acid moiety, as represented in Table 1.

More into details, xylan DTG curves displayed an initial major dual-stage peak, with maxima centred at 255 °C and 290 °C at 3 °C/min (Fig. 3B). Shen et al. in [29] associated the first DTG peak to the cleavage of the glycosidic bonds and to the decomposition of side-chain structures like the methyl-glucuronic acid, and the second peak to fragmentation of the xylan units. Upon increasing the heating rate, the pyrolysis shifted to higher temperatures and the intensity of the first peak grew, in line with with previous literature studies performed under similar conditions [28,29,34,46,50].

After this primary mass loss step, xylan exhibited a secondary devolatilization stage resulting in a slope change in TG curves. At 3 °C/min this secondary stage occurred around 350 °C, at 100 °C/min around 400 °C (Fig. 2A and E). The solid residual was significantly higher than that observed with cellulose, and it decreased upon increasing the heating rate. Additionally, in contrast to cellulose, xylan TG curves showed a smooth declining trend until the end of the tests. This evidence suggests the onset of charring reactions at temperature as low as 300 °C and the consecutive release of species in the vapour phase [16,29].

A single-stage primary mass loss was instead seen in the case of

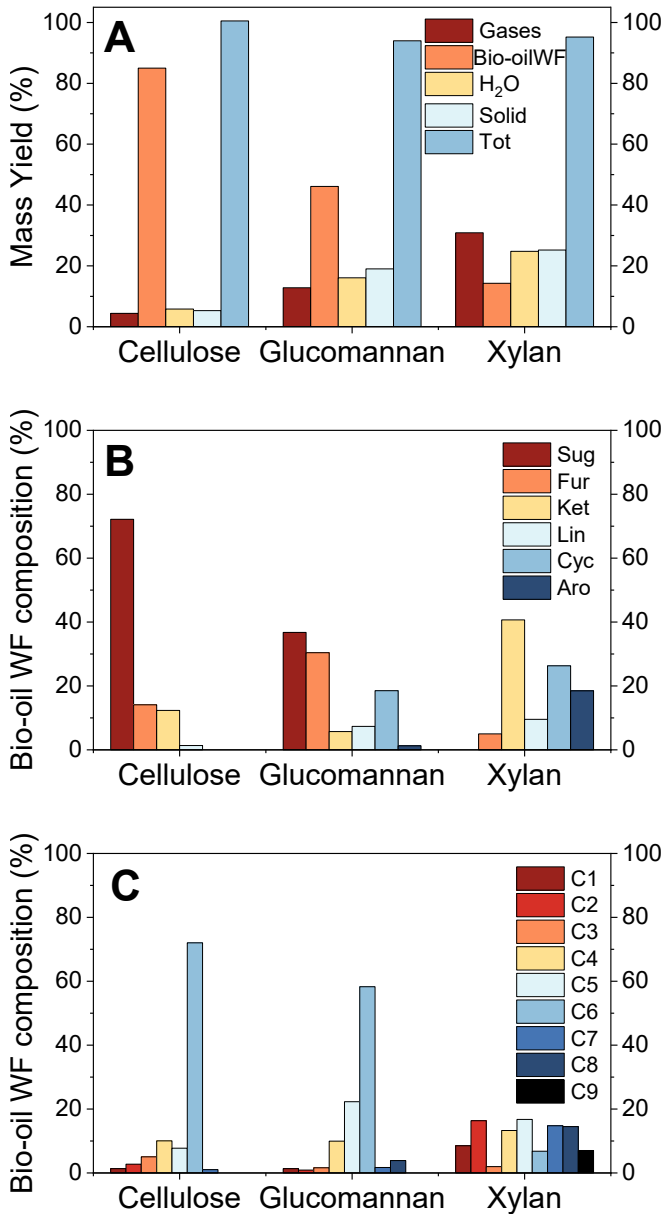

Fig.3. Product speciation from cellulose, xylan and glucomannan pyrolysis in TGA at 100 °C/min: overall yields (A) and bio-oil composition (B-C). Sug = anhydrosugars, monosaccharides; Fur = furanic species; Ket = aliphatic ketones and aldehydes; Lin = aliphatic alcohols, carboxylic acids, anhydrides, ethers; Cyc = cyclic oxygenates; Aro = aromatics.

glucomannan, that exhibited a behaviour more similar to cellulose, due to their similar chemical structure based on hexose unit. In fact, DTG curves showed a major single devolatilization peak, shifting from 290 °C at 3 °C/min to 350 °C/min at 100 °C/min (Fig. 2B, F), representing the primary devolatilization stage. Similar to xylan, glucomannan exhibited a secondary devolatilization stage, as well as a continuous declining trends of TG curves. In terms of solid residual, glucomannan values fell between those of xylan and cellulose. Similar TG and DTG trends were observed by Moriana et al. testing a glucomannan extracted from spruce wood [27].

In conclusion, xylan and glucomannan have revealed distinct devolatilization trends, confirming the significance of individual examination. Besides, this investigation reveals that the devolatilization process of glucomannan is intermediate between those of cellulose and xylan.

3.2. Detailed product speciation with TGA-based methodology

The complete quantitative speciation of the products obtained from xylan and glucomannan pyrolysis was achieved using our in-house developed TGA-based methodology and following the optimized procedures presented in section 2.2. Also in this case, cellulose pyrolysis was used as a reference. The primary objective was to associate each model biomass to a specific integral product slate and to highlight the characteristic features. The combination of the thermogravimetric curves at varying heating rates (covering an extended temperature range) and the detailed speciation provides a dataset of the highest value for the kinetic modelling of the pyrolysis process.

The optimized protocol for speciation consists of a TGA run with a heating rate of 100 °C/min, a condition that allows to shorten the duration of the experiment and to rapidly release pyrolysis products in a pulse-like manner.

3.2.1. Product distribution in gas, liquid and solid streams

Fig. 3(A) presents the yields of various product streams, i.e., gases, water, bio-oil and solid residue. The term "bio-oil$_{WF}$" (water-free bio-oil) includes the entire group of condensable species, with the exclusion of H_2O. Remarkable mass balances were achieved, with integral mass yields summing up to 100.5 %, 95.2 % and 94.0 % for cellulose, xylan and glucomannan, respectively. This significant outcome serves as strong evidence supporting the effectiveness of this TGA-methodology for the study of biomass pyrolysis kinetics.

Cellulose maximized the yield of the organic liquid fraction (bio-oil$_{WF}$). Conversely, xylan products were distributed nearly evenly among the different categories of solid residual, gases and condensable products.

Glucomannan displayed an intermediate behaviour, with yields of gases, liquid and solid of 12.8 %, 62 % (including 16.1 % of H_2O and 46.1 % of bio-oil$_{WF}$) and 19.0 %, respectively.

3.2.2. Composition of bio-oil

Table 2 reports the integral mass yields of each single species measured during experiments of cellulose, xylan and glucomannan; also in this case, the reader is referred to [37] for a detailed discussion on cellulose case, that in this work served as reference case for comparison of hemicellulose behaviour. The molecular structure of identified species is reported in Table S3 in the Supplementary Material (section S.3). Bio-oil from glucomannan and xylan pyrolysis contained a wide group of oxygenated species, comprising anhydrosugars, monosaccharides, furanic compounds, other cyclic oxygenated species, aromatic compounds, aliphatic ketones, aldehydes, carboxylic acids and ethers. While the case of cellulose is dominated by C_6-anhydrosugars products, among which levoglucosan prevailed with a yield of 47.6 %, the broad group of condensable products produced by the two hemicelluloses here investigated is characterized by a variety of species, each contributing with a modest share in terms of integral mass yield. Specifically, 30 and 43 condensable oxygenates were identified and quantified in the case of xylan and glucomannan pyrolysis, respectively.

For a clearer depiction of product distribution, Fig. 3 presents bio-oil composition in terms of classes of products, grouped according to their chemical functionality (Fig. 3(B)) or the length of C-chain (Fig. 3(C)).

In the case of xylan, aliphatic ketones constituted the main class of condensable products, followed by cyclic oxygenates and aromatic species. This distribution spanned homogeneously across the C_1-C_9 range. None anhydrosugars were detected and the dominance of C_5 species was not observed. This is in strong contrast to cellulose, where the most important product, levoglucosan LVG, was the equivalent of its C_6 monomeric unit (being xylan a pentose-based polymer the release of the monomeric unit would result in a strong product of C_5). Besides H_2O, key products were light species like methanol and acetaldehyde. The presence of aromatic compounds indicated a contamination of the xylan powder from lignin-structures. Nonetheless, the overall yield to the

Table 2
Product distribution in TGA experiments.

	Formula	Integral mass yield [%] Cellulose	Xylan	Glucomannan
Mass balance		100.5	95.2	94.0
Gases				
Carbon monoxide	CO	1.7	9.0	4.6
Carbon dioxide	CO_2	2.5	20.2	7.7
Methane	CH_4	0.2	1.3	0.3
C_2H_x	C_2H_x	–	0.4	0.2
Anhydrosugars, monosaccharides				
DL-Arabinose	$C_5H_{10}O_5$	0.1	–	–
Levoglucosenone (LGO)	$C_6H_6O_3$	1.5	–	0.6
1,4:3,6-dianhydro-α-D-glucopyranose (DGP)	$C_6H_8O_4$	1.4	–	1.7
3,4-Anhydro-d-galactosan	$C_6H_8O_4$	0.6	–	–
2,3-Anhydro-d-mannosan	$C_6H_8O_4$	0.9	–	1.0
Levoglucosan (LVG)	$C_6H_{10}O_5$	47.6	–	9.8
1,6-anhydro-β-D-glucofuranose	$C_6H_{10}O_5$	3.8	–	–
2-Deoxy-D-galactose	$C_6H_{12}O_5$	3.6	–	–
D-Allose	$C_6H_{12}O_6$	0.8	–	4.6
Furans				
Furan	C_4H_4O	4.6	0.1	<0.1
2(5H)-Furanone	$C_4H_4O_2$	–	–	0.5
2(3H)-Furanone, dihydro-4-hydroxy-	$C_4H_4O_3$	–	–	0.3
2,3-dihydrofuran	C_4H_6O	0.5	–	–
3-Furaldehyde	$C_5H_4O_2$	0.3	–	–
Furfural	$C_5H_4O_2$	2.4	0.1	0.4
2-Furanmethanol	C_5H_6O	–	–	3.4
2-methylfuran	C_5H_6O	2.2	<0.1	0.4
3-Methyl-2(5H)-furanone	$C_5H_6O_2$	–	0.1	–
2-Furanmethanol, tetrahydro-	$C_5H_{10}O$	–	–	1.4
2-Furanol, tetrahydro-2-methyl-	$C_5H_{10}O_2$	–	–	0.2
2-Vinylfuran	C_6H_6O	0.4	–	
5-Hydroxymethylfurfural	$C_6H_6O_3$	–	–	3.0
2,5-dimethylfuran	C_6H_8O	0.6	–	0.2
Furaneol	$C_6H_8O_3$	–	–	1.0
2-Furaldehyde, 5-methyl	$C_6H_6O_2$	–	–	0.4
2-Acetylfuran	$C_6H_6O_2$	–	–	1.7
2-Allylfuran	C_7H_8O	–	<0.1	–
2-propylfuran	$C_7H_{10}O$	0.9	–	–
5-acetoxymethyl-2-furaldehyde	$C_8H_8O_4$	–	–	1.8
Ketones, aldehydes				
Formaldehyde	CH_2O	1.2	<0.1	<0.1
Acetaldehyde	C_2H_4O	1.7	2.3	<0.1
Hydroxy-acetaldehyde (HAA)	$C_2H_4O_2$	0.7	–	<0.1
Acetone	C_3H_6O	3.9	0.3	<0.1
Hydroxy-acetone	$C_3H_6O_2$	0.4	–	0.7
Succinaldehyde	$C_4H_6O_2$	–	–	0.4
2-butanone	C_4H_8O	–	0.4	–
2,3 Butanedione	$C_4H_6O_2$	2.4	0.7	0.3
2,3 Pentanedione	$C_5H_8O_2$	–	0.4	0.5
Glutaraldehyde	$C_5H_8O_2$	0.2	–	0.7
3-Hexanone	$C_6H_{12}O$	–	0.2	–
3,4-Hexanedione	$C_6H_{10}O_2$	–	<0.1	–
Cyclic oxygenates				
Dioxene	$C_4H_6O_2$	–	–	–
Butyrolactone	$C_4H_6O_2$	–	–	0.4
2-Hydroxy-gamma-butyrolactone	$C_4H_6O_3$	–	0.3	1.0
1,2-Cyclopentanedione	$C_5H_6O_2$	–	–	1.5
Cyclopentanol	$C_5H_{10}O$	–	0.7	2.6
1,2-Cyclopentanediol	$C_5H_{10}O_2$	–		0.6
2,2-Dimethyl-1,3-dioxane-4,6-dione	$C_6H_8O_4$	–	–	–
2-Cyclohexenol	$C_6H_{10}O$	–	–	0.8
1,2-Cyclopentanedione, 3-methyl-	$C_6H_8O_2$	–	0.3	0.9
1,4-Dioxaspiro[2,4]heptan-5-one, 7-methyl	$C_6H_8O_3$	–	–	0.7
2-Cyclopenten-1-one, 3,4-dimethyl-	$C_7H_{10}O$	–	<0.1	–
Ethylcyclopentenolone	$C_7H_{10}O_2$	–	–	0.8
4,4-Dimethyl-2-cyclopenten-1-one	$C_7H_{10}O$	–	<0.1	–
1,2-Dioxolan-3-one, 5,5-diethyl-4-methylene-	$C_8H_{12}O_3$	–	1.42	–
Carboxylic acids, anhydrides, ethers, alcohols				
Methanol	CH_4O	–	1.1	0.6
Acetic acid	$C_2H_4O_2$	–	–	0.3
Acetic anhydride	$C_4H_6O_3$	1.1	–	
Methyl pyruvate	$C_4H_6O_3$	–	–	0.5
Ethyl-1-propenyl ether	$C_5H_{10}O$	–	0.3	–
Pivalic acid	$C_5H_{10}O_2$	–	0.7	–
Aromatics				
Catechol	$C_6H_6O_2$	–	0.4	0.6
Benzyl alcohol	C_7H_8O	–	<0.1	–
1,2-Benzenediol, 3-methyl-	$C_7H_8O_2$	–	0.9	–
2,3-Dihydroxybenzaldehyde	$C_7H_6O_3$	–	0.9	–
Phenol, 2,5-dimethyl-	$C_8H_{10}O$	–	0.2	–
Resorcinol, 2-acetyl-	$C_8H_8O_3$	–	0.4	–
6-Hydroxy-3,4-dihydrocoumarin	$C_9H_8O_3$	–	1.0	–
Others				
3-Pyrazolidinone, 1,4-dimethyl	$C_5H_{10}N_2O$	–	0.4	–
Cyclopentadiene	C_5H_6	1.4	–	–

organic bio-oil fraction remained confined to 14.3 %. Notably, acetic acid was not detected in this study: it is known that acetic acid is primarily produced from the 2-O-acetyl xylopyranose cleavage [14,51]. Its absence in this study might suggest a leakage of acetyl side groups in the commercial xylan under investigation, although we cannot exclude that acetic acid could not be detected when present in trace amounts.

In contrast to xylan, glucomannan gave a superior yield of organic bio-oil fraction. Anhydrosugars and furanic compounds emerged as most important fractions, followed by other cyclic oxygenates. Like cellulose case, levoglucosan was the most important product, indicating the significant impact of monomeric unit release. Alongside levoglucosan, products like D-allose, DGP (1,4:3,6-dianhydro-α-D-glucopyranose), hydroxy-methylfurfural and acetylfuran made the class of C_6 species the one with the highest integral mass yield. Other important products were cyclopentanol, cyclopentanedione, furanmethanol and tetrahydrofuranmethanol (all C_5).

3.2.3. Composition and evolution of gas products

Table 2 indicates that, similarly to cellulose, CO and CO_2 were the main gaseous products from xylan and glucomannan pyrolysis, in agreement with literature findings from TGA-FTIR tests [34]. Furthermore, trace quantities of methanol, methane and of C_2 hydrocarbons (ethane, ethylene) were also detected. The monitoring of these gaseous species coupled with TG trends is shown in Fig. 4 for xylan and glucomannan cases. For both hemicelluloses, the primary devolatilization step was accompanied by the generation CO and CO_2. In the case of xylan, their production pattern reflected the dual-stage nature of xylan devolatilization, nonetheless with some signal resolution challenges due to the short duration of the experiment with this heating rate of 100 °C/min. Conversely, single distinct peaks of CO_2 and CO were observed for glucomannan. The secondary devolatilization stage (section 3.1) was instead associated to the release of CH_3OH and CH_4, together with a residual production of CO_x species. Notably, a tertiary minor release of CH_4 and C_2 species was observed at higher temperature, where TG curves were following a gradual decline, likely related to charring reactions as discussed in section 3.1. The high temperature production of

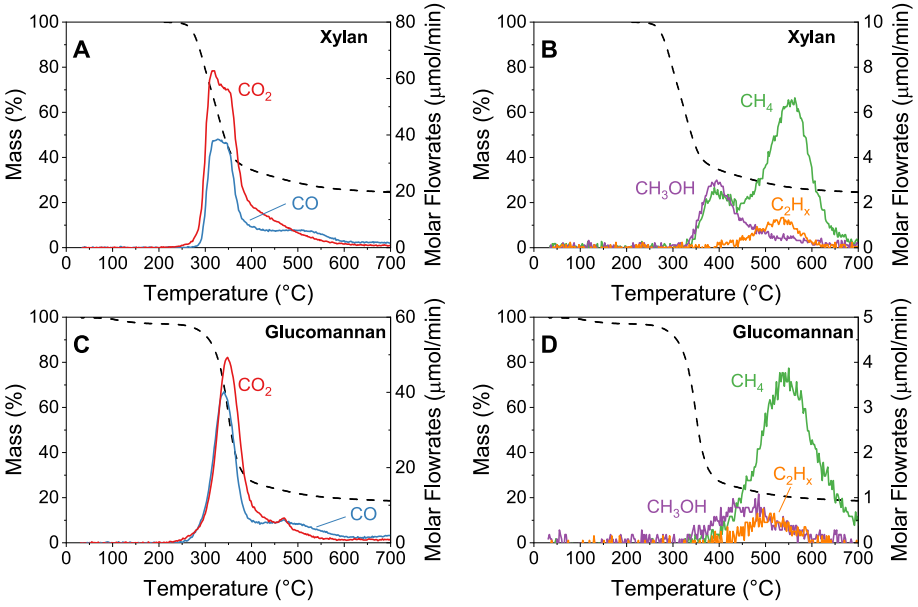

Fig.4. Online monitoring of CO_x, CH_4, C_2H_x and CH_3OH during xylan (A-B) and glucomannan (C-D) pyrolysis at 100 °C/min. Dashed lines = TG curves (left y-axis); solid lines = gas molar flowrates (right y-axis).

methane has been already associated to the onset of charring reactions in the literature [31,34].

The online quantification of gases and H_2O allows to calculate (upon integration) the real-time yields of these species, according to Eq. (1). Notably, the Orbo traps partially delay the flow of H_2O, causing an experimental uncertainty in its real-time monitoring at high heating rate [37]. Fig. 5 associates the mass loss curves with the product distribution: this information coupled with the detailed composition measurement of bio-oil species provides a kinetic insight of key importance.

3.2.4. *Kinetic insight*

Discussion on the mechanism of hemicellulose pyrolysis is already present in the literature, primarily focused on xylan: there is a general agreement that the devolatilization process begins with a dehydration stage, associated with the decomposition of unstable side chain groups (e.g., acetyl-chain groups). This is followed by the breakdown of the polysaccharide chain, involving both primary depolymerization, releasing the monosaccharide, and secondary fragmentation routes that form other oxygenates [14,49,52].

The results presented in this work provide the quantitative details necessary to support and formalize these mechanistic investigations.

Fig. 6 rationalizes and combines the insights gained from TG curves (Fig. 2) and products analysis (Fig. 3). Three main pyrolysis routes were identified and their relative importance in the case of cellulose, xylan and glucomannan was quantified: i) depolymerization with release of monomeric unit (C_6 anhydrosugars for cellulose and glucomannan; C_5 anhydrosugars for xylan); ii) formation of other oxygenated fragments (C_1-C_6); iii) route to gas, H_2O and char.

The simultaneous analysis of conversion and product distribution reveals that the route to gas, H_2O and char gains importance at decreasing thermal stability (that follows the order xylan < glucomannan < cellulose), justifying a yield of only 15 % in the case of cellulose up to 85 % for xylan.

Then the closure of mass balance and the detailed speciation of bio-oil compounds allow to quantify the relative weight of the depolymerization reaction vs the fragmentation reaction. The devolatilization of hexose-based polysaccharides result in a significant yield of C_6 anhydrosugars (50 % for cellulose, 20 % for glucomannan), mirroring an important role of the depolymerization route. In contrast, the route to C_5 anhydrosugar is inactive in the case of xylan, indicating an easier cleavage of the monomeric unit. The route to oxygenates fragments accounts for yields of approximately 15 % for xylan, 30 % for glucomannan and 35 % for cellulose; the detailed and quantitative product speciation will eventually open to the development of reaction stoichiometries.

Interestingly, glucomannan showed a behaviour intermediate between cellulose and xylan. This is attributed to its intermediate chemical structure, as glucomannan is a fully amorphous polysaccharide like xylan, but is hexose–based like cellulose.

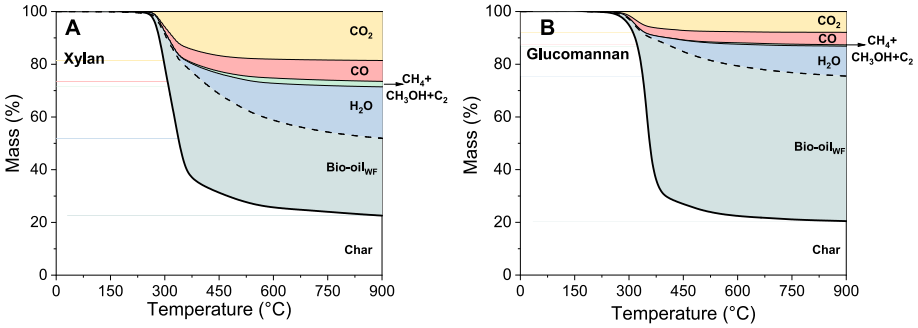

Fig.5. TG curves and product distribution measured during the pyrolysis of xylan (A) and glucomannan (B) at 100 °C/min. Gases and H_2O profiles were calculated from concentration vs. time plots; bio-oil is shown as complement to close mass balances.

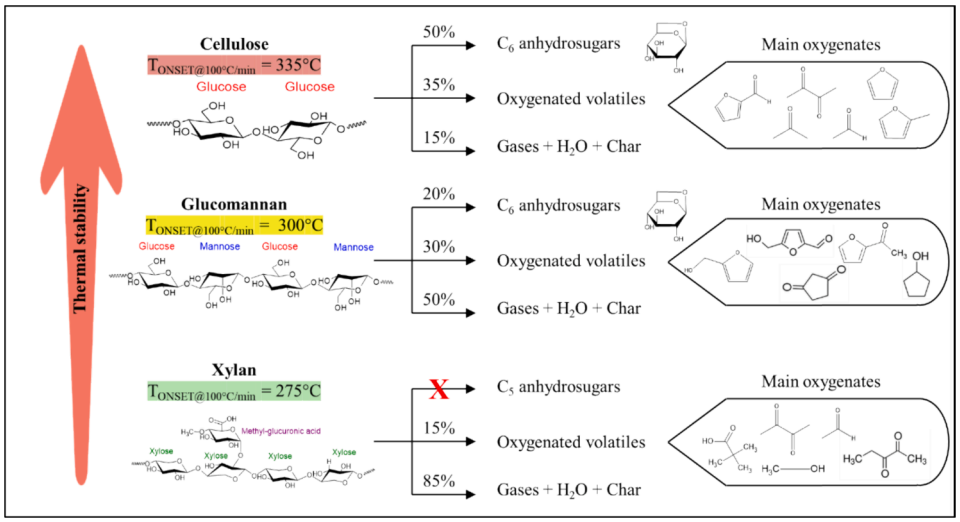

Fig.6. Measured onset temperatures at 100 °C/min, identified devolatilization routes with their relative weight and main detected oxygenates for cellulose, glucomannan and xylan pyrolysis.

3.3. Comparison with model predictions

The investigation in TGA has revealed substantial differences in the behaviour of the three biomass macro-constituents, clearly highlighting a disparity not only between cellulose and hemicellulose, but also within different hemicellulosic polysaccharides. Hence, these findings underline the crucial importance of performing independent studies on the devolatilization kinetics of these macro-constituents.

The great novelty of these datasets relies in their comprehensiveness, with the combined obtainment (for each model biomass) of information on the rate and the distribution of entire spectrum of gaseous, liquid and solid products of pyrolysis.

To better appreciate the potential behind such information, we herein compare the experimental evidence with the predictions of two state-of-the-art lumped schemes [16,26], that were trained against datasets from various biomasses; in the specific case of hemicellulose pyrolysis, where the available information has been partial and fragmentary, a higher reliability of the models' response is expected about the simulation of TG curves, but more uncertain will be the response about whole product distribution, typically not available from the literature.

3.3.1. TG curves

Model predictions of TG and DTG curves from cellulose, xylan and glucomannan are shown in Fig. 2 and compared with experimental measurements observed under varying heating rates. This paragraph will focus on the predictions of xylan and glucomannan devolatilization, since the case of cellulose has already been discussed [37].

As expected, the predictions of the two models are extremely similar. In general, a very good agreement between model predictions and experimental curves is observed in Fig. 2 for both xylan and glucomannan. Although predicted TG curves exhibit plateaus that are not seen experimentally – due to the discretization inherent to the lumping process – DTG curves show that the devolatilization events predicted by the model align with the experimental ones.

The two models predict the devolatilization curves within the correct temperature windows, and well distinguish the dual-stage pyrolysis of xylan and the single-stage pathway of glucomannan.

The model of Debiagi et al. [26] is also able to describe the secondary devolatilization stage, with a clearly visible peak in DTG curves (centred for instance at 340 °C at 3 °C/min). The greatest discrepancy is seen at elevated temperatures, where this model strongly overestimates the observed mass loss, which was instead little pronounced. Instead, the model of Dussan et al. [16] better match the final char yields.

3.3.2. Product distribution

Fig. 7 compares the yields of product streams predicted by model simulations with experimental measurements in TGA at 100 °C/min. For model simulations, the integral yields were calculated up to 600 °C. Fig. 7(A-B) show the yields of overall product streams in xylan and glucomannan pyrolysis: as expected, significant differences emerge between the two models, proving the lack of consolidated knowledge on the kinetics of hemicellulose pyrolysis. In the case of xylan, the model of Dussan et al. [16] well describes the distribution of products in the different streams, while that of Debiagi et al. [26] largely overestimates bio-oil$_{WF}$ and underestimates H_2O. For glucomannan, both the models overrate gases, and also the predictions of liquid yields are not satisfactory.

More detailed considerations can be done by analysing the integral yields of single species.

Predictions of bio-oil compositions are compared with experimental measurements in Fig. 7(C-F): the two models provide significantly different predictions, again proving the weakness of the initial experimental databank. In both cases, large margins of improvement clearly emerge.

In the case of xylan, the model of Debiagi et al. [26] fails to depict the uniform distribution of products across the C_1-C_9 range, and predicts a predominance of anhydrosugar and furanic species. However, these model predictions diverge from experimental observations, where anhydrosugar compounds were not detected, in line with other studies [28,47,53,54]. Instead, the model of Dussan et al. [16] overestimates C_2 and C_3 products and furans.

In the case of glucomannan, species C_5 and C_6, owning to the classes of anhydrosugars or furanic compounds, prevail both in the experiments and model predictions of Debiagi et al. [26]; instead, the model of Dussan et al. [16] does not include C_5 products. Light species C_1 and C_2 are overestimated by both models, while cyclic oxygenates are not accounted among model products.

Overall, this analysis uncovers the existence of notable room for improvement in the prediction of pyrolysis products distribution. The newly collected data with the present TGA-based methodology are thus able to provide kinetic insights on both devolatilization rates and product distribution. These findings are of great use to guide the kinetic scheme refinement.

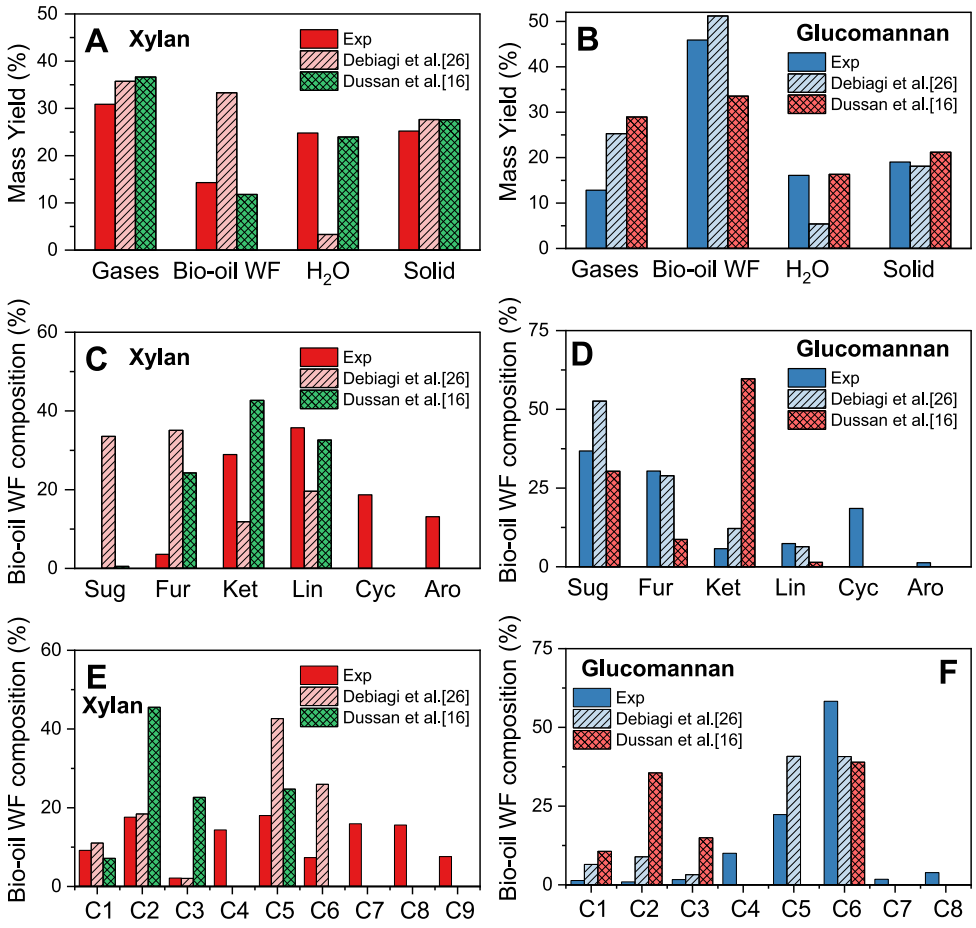

Fig.7. Product speciation from xylan (A, C, E) and glucomannan (B, D, F) pyrolysis at 100 °C/min: a comparison of experimental measurements and model predictions [16,26]. Sug, Fu, Ket, Lin, Cyc, Aro: defined as in Fig. 3.

3.4. *Pyrolysis tests in fixed bed reactor*

Pyrolysis experiments in the fixed bed reactor were carried out to explore scales more representative than the TGA. Fig. 8 shows speciation results obtained from cellulose, xylan and glucomannan pyrolysis at 500 °C, in terms of overall yields to product streams and mass balances (Fig. 8(A)), and the bio-oil composition (Fig. 8(B-C)). The complete list of integral yields of each individual species is reported in the Table S4 in the Supplementary Material (section S.4). Importantly, mass balances were not fully closed in the case of cellulose and glucomannan: indeed, the presence of significant condensation in the lines upstream from the condenser where the liquid fraction was collected, suggested that the unaccounted portion pertains to condensable products. Therefore, this indication suggests a higher production of bio-oil from cellulose and glucomannan in comparison to the measured values.

3.4.1. *Product speciation*

At 500 °C, cellulose exhibited the highest yield of bio-oil, while the yields of gas, H_2O and solid residual were all limited. The greatest solid residual was achieved by xylan, whose products were evenly distributed among the different categories (27.0 % yield of gases, 23.1 % of H_2O, 30.6 % of bio-oil). Similar overall yields for xylan were observed by Stefanidis et al. in [28] during similar experiments in fixed bed reactor at 500 °C. Glucomannan displayed an intermediate behaviour in terms of gas and solid yields, while bio-oil and H_2O closely resembled the ones from xylan. This intermediate behaviour is consistent with its hybrid chemical identity, comprising C_6 monomeric units, but lacking the typical crystallinity observed in cellulose. The uncomplete closure of mass balances points out an even more pronounced tendency of cellulose towards bio-oil production, and indicates an intermediate behaviour of glucomannan also in terms of bio-oil production.

The speciation protocol described in section 2.3 allowed to accurately determine the integral mass yield of each individual species. Among gas products, CO and CO_2 were the predominant species in all the tests, while light hydrocarbons were detected only in traces amounts. A more complex scenario emerged instead considering bio-oil composition, which was characterized by a large number of species: 45 condensable volatiles were identified for cellulose and for xylan, and 50 for glucomannan. For a better understanding, the species found in bio-oil were grouped based on their chemical functionality in Fig. 8(B) and their C-chain length in Fig. 8(C), as already done in the case of TG experiments (Fig. 3).

Cellulose bio-oil was marked by the presence of C_6 anhydrosugar products, among which levoglucosan emerged as the most important product. Furanic species and aliphatic ketones were also detected, distributed among species within the range of $C_1 - C_5$.

In contrast, xylan showed minimal presence of anhydrosugars, while aliphatic ketones, carboxylic acids and alcohols represented the most important products. These products spanned evenly from C_1 to C_6 species, with notable components including methanol, hydroxy-butanone, hydroxy-acetone, propionic anhydride, propanoic acid, furfural, acetic anhydride, methacrolein and hydroxy-acetaldehyde. These finding corroborate the absence of anhydrosugars observed in TGA tests.

In accordance with the trend observed for overall yields, glucomannan showed an intermediate behaviour between cellulose and hemicellulose: like cellulose, C_6 anhydrosugars were the most abundant class of products. Furanic species and aliphatic ketones were detected in comparable quantity, alongside lower amount of cyclic oxygenates and

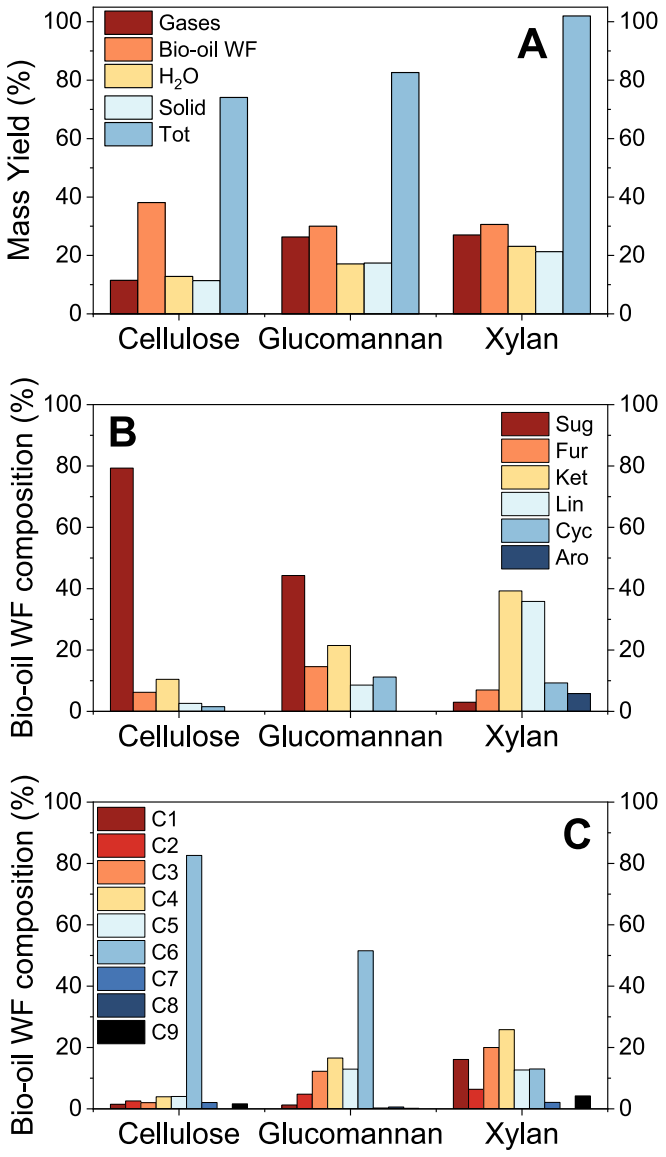

Fig.8. Product speciation from the pyrolysis of cellulose, xylan and glucomannan in fixed bed reactor at 500 °C (A, C, E) and 550 °C (B, D, F). Sug, Fu, Ket, Lin, Cyc, Aro: defined as in Fig. 3.

aliphatic acids. The most important products were levoglucosan, D-allose, hydroxy-acetone, hydroxy-acetaldehyde, acetic anhydride and hydroxy-methylfurfural.

Pyrolysis tests were repeated at 550 °C and speciation results are displayed in Fig.S1 in the Supplementary Material (section S.5). Notable variations were detected only in the composition of bio-oils from cellulose and glucomannan, where the increase in temperature lead to a reduction of anhydrosugars and increased C_1-C_5 oxygenates, while no impact was observed for xylan pyrolysis.

To complete this comparative study on the pyrolysis of cellulose, xylan and glucomannan, char samples obtained from experiments in fixed bed reactor were analysed using Raman spectroscopy and TPO measurements. Fig.S2 in the Supplementary Material (section S.6) presents Raman spectra obtained from char samples from pyrolysis at 550 °C, while Fig.S3 (section S.7) shows the mass loss trends and the DTG curves measured during TPO. These analyses revealed the presence of both graphitic and amorphous carbon in all the char samples, but chars from hemicellulose pyrolysis exhibited a lower presence of structured C-species compared to cellulose. This less structured form of hemicellulosic char samples turned into a lower thermal stability during TPO. Moreover, back-calculations allowed to estimate the ash content with respect to the initial weight of biomass, that amounted to 2.6 % for both the hemicelluloses and to 0.2 % for cellulose.

3.4.2. *Comparison of TGA and fixed bed experiments*

The comparison of results of TGA and fixed bed experiments is not straightforward due to the inherent difference between the two systems, since TGA tests followed a temperature ramp, whereas fixed bed experiments were isothermal. Given the key role of temperature in pyrolysis, this disparity is expected to lead to variations in the product distribution. Moreover, the dynamic heating of the biomass sample and the potential onset of heat transfer limitations impact fixed bed experiments, leading to a more complex and less predictable temperature profile within the biomass bed. Despite these factors preventing a strict comparison, an integrated analysis of results from the two systems is extremely valuable to establish common trends and to analyse the impact of the different feedstocks on product distribution.

Notably, the results from TGA are anyway aligned with the trends observed in fixed bed reactor: cellulose showed the lowest yield of solid residual and highest yield of bio-oil, and the C_6 anhydrosugar LVG was the most important product. Also for the two hemicelluloses, experiments at both scales provided the same picture: xylan exhibited the largest solid residue, with products being evenly distributed among the solid, liquid and gas phases. Condensable oxygenates spanned homogeneously across the C_1-C_9 range and different chemical functionalities, without the emergence of C_5 species and anhydrosugars.

Glucomannan showed a behaviour intermediate between cellulose and xylan. The significant production of levoglucosan also in the case of glucomannan, indicates that release of a C_6 unit is more favoured than that of a C_5 unit, where fragmentation routes prevail. Again, these features arose both from fixed bed and TGA experiments. Accordingly, experiments carried out in fixed bed equipment validate the observations obtained from the ideal TGA setup.

Therefore, experiments in TG and fixed bed reactor provided complementary results: fixed bed tests allowed to explore pyrolysis on a more representative scale (e.g. sample weight of 500 mg vs 10 mg in TGA), of great importance for measuring global performance indicators. However, the potential onset of transfer limitations and the dynamic heating of the sample challenge the description of the temperature evolution inside the biomass sample. Due to these complexities, as well as the possible impact of secondary reactions, an inclusive reactor model would be essential for extracting kinetic information from these experiments. On the contrary, the controlled TGA setup allowed for the collection of kinetic relevant data, useful for the evaluation of reaction schemes and kinetic parameters.

4. Conclusions

The development of chemical reaction engineering of hemicellulose pyrolysis has been traditionally hampered by the scarcity, the fragmentation and qualitative nature of experimental data. Indeed, in any complex reacting system, if conversion measurements are not accompanied by the simultaneous quantification of all the products, the identification of reaction stoichiometries and chemical pathways remains open. The existing lumped kinetic schemes have addressed the issue by sewing independent pieces of information of diverse prevenience and qualitative nature.

In this work, for the first time, conversion measurements of xylan and glucomannan were collected together with detailed product speciation; a quantitative approach was applied and allowed to reach the unique result of closure of mass balances. In particular, more than 40 condensable species were detected and individually quantified, thus providing an extremely precise definition of bio-oil composition.

Experiments with the TGA-methodology revealed the peculiar features of hemicellulose vs cellulose and of xylan vs glucomannan. Cellulose displayed a high-temperature single-step devolatilization, with

high bio-oil yield. The C_6 anhydrosugar levoglucosan was the most important product, proving the key role of monomeric unit release during devolatilization.

Xylan pyrolysis was characterized by a primary dual-step devolatilization, a secondary devolatilization stage and finally the onset of charring reactions. Products were almost evenly distributed among the solid, liquid and gas streams; condensable oxygenates spanned homogeneously across the C_1-C_9 range. Aliphatic and cyclic oxygenates of various classes were detected, but notably anhydrosugars were absent, demonstrating a substantial deviation from cellulose in devolatilization pathways and a stronger fragmentation tendency within the monomeric unit.

Glucomannan exhibited an intermediate chemical behaviour between cellulose and xylan, in terms of devolatilization trend, solid residual and product distribution. This mirrors its hybrid chemical structure, being glucomannan a fully amorphous polysaccharide like xylan, but hexose–based like cellulose. Therefore, glucomannan pyrolysis showed a primary devolatilization stage that was single-step like cellulose, but a secondary devolatilization stage and charring reactions were also observed likewise the xylan case. Like cellulose, LVG was the most important product but other furanic, aliphatic and cyclic oxygenates were also present in significant amount.

Experiments in fixed bed reactor allowed to collect complete speciation of pyrolysis products on more representative scales, thus further enriching the databank on hemicellulose, that is extremely scarce in the current literature, in particular for glucomannan. Notably, speciation results from TGA-setup and fixed bed reactor mostly aligned, thus further validating the approach. Moreover, experiments in fixed bed allowed the collection of char samples and their characterization: in general, a higher stability and a lower ash content was observed in the case of char from cellulose pyrolysis.

The predictions of two state-of-the-art lumped kinetic models were compared with experimental data and significant margins of improvement were identified, in particular for the product speciation, whose refinement will need the partial de-lumping of species. At the best of the authors' knowledge, this work provides a unique dataset for the advancement of pyrolysis modelling, a key phase towards technology progress.

CRediT authorship contribution statement

Veronica Piazza: Writing – original draft, Methodology, Investigation, Data curation. **Roberto Batista da Silva Junior:** Methodology, Investigation. **Alessio Frassoldati:** Writing – review & editing, Supervision. **Luca Lietti:** Writing – review & editing, Supervision. **Chiara Gambaro:** Supervision. **Kishore Rajendran:** Investigation. **De Chen:** Supervision. **Tiziano Faravelli:** Writing – review & editing, Supervision, Conceptualization. **Alessandra Beretta:** Writing – review & editing, Supervision, Methodology, Funding acquisition, Conceptualization.

Declaration of competing interest

The authors declare that they have no known competing financial interests or personal relationships that could have appeared to influence the work reported in this paper.

Data availability

Data will be made available on request.

Acknowledgements

This research has received funding from ENI S.p.A. (PhD scholarship to V. Piazza) and from Dipartimento di Energia, Politecnico di Milano, within *Energy for Motion* Dipartimenti Eccellenti-MIUR funding program. This study was partially conducted within the Agritech National Research Center and received funding from the EU Next-GenerationEU (PNRR) – MISSIONE 4 COMPONENTE 2, INVESTIMENTO 1.4 and 1.3 – D.D. 1032 17/06/2022, CN00000022). This manuscript reflects only the authors' views and opinions, neither the EU nor the EC can be considered responsible for them.

Appendix A. Supplementary data

Supplementary data to this article can be found online at https://doi.org/10.1016/j.cej.2024.154579.

References

[1] A.K. Vuppaladadiyam, S.S.V. Vuppaladadiyam, A. Awasthi, A. Sahoo, S. Rehman, K.K. Pant, S. Murugavelh, Q. Huang, E. Anthony, P. Fennel, S. Bhattacharya, S. Y. Leu, Biomass pyrolysis: A review on recent advancements and green hydrogen production, Bioresour. Technol. 364 (2022), https://doi.org/10.1016/j.biortech.2022.128087.

[2] S. Pang, Advances in thermochemical conversion of woody biomass to energy, fuels and chemicals, Biotechnol. Adv. 37 (2019) 589–597, https://doi.org/10.1016/j.biotechadv.2018.11.004.

[3] G. Velvizhi, K. Balakumar, N.P. Shetti, E. Ahmad, K. Kishore Pant, T. M. Aminabhavi, Integrated biorefinery processes for conversion of lignocellulosic biomass to value added materials: Paving a path towards circular economy, Bioresour. Technol. 343 (2022), https://doi.org/10.1016/j.biortech.2021.126151.

[4] J. Alvarez, G. Lopez, M. Amutio, J. Bilbao, M. Olazar, Bio-oil production from rice husk fast pyrolysis in a conical spouted bed reactor, Fuel 128 (2014) 162–169, https://doi.org/10.1016/j.fuel.2014.02.074.

[5] A. Arregi, M. Amutio, G. Lopez, J. Bilbao, M. Olazar, Evaluation of thermochemical routes for hydrogen production from biomass: A review, Energy Convers. Manag. 165 (2018) 696–719, https://doi.org/10.1016/j.enconman.2018.03.089.

[6] A. Arregi, G. Lopez, M. Amutio, I. Barbarias, J. Bilbao, M. Olazar, Hydrogen production from biomass by continuous fast pyrolysis and in-line steam reforming, RSC Adv. 6 (2016) 25975–25985, https://doi.org/10.1039/c6ra01657j.

[7] D. Lee, H. Nam, M. Won Seo, S. Hoon Lee, D. Tokmurzin, S. Wang, Y.K. Park, Recent progress in the catalytic thermochemical conversion process of biomass for biofuels, Chem. Eng. J. 447 (2022), https://doi.org/10.1016/j.cej.2022.137501.

[8] M. Mujtaba, L. Fernandes Fraceto, M. Fazeli, S. Mukherjee, S.M. Savassa, G. Araujo de Medeiros, A. do Espírito Santo Pereira, S.D. Mancini, J. Lipponen, F. Vilaplana, Lignocellulosic biomass from agricultural waste to the circular economy: a review with focus on biofuels, biocomposites and bioplastics, J. Clean. Prod. 402 (2023), https://doi.org/10.1016/j.jclepro.2023.136815.

[9] A. Villot, J. Pena, C. Gerente, Recovery of pyrolysis char from residual biomass in accordance with the principles of the circular economy, Fuel 331 (2023), https://doi.org/10.1016/j.fuel.2022.125837.

[10] Y.H. Chan, S.S.M. Lock, B.L.F. Chin, M.K. Wong, A.C.M. Loy, S.Y. Foong, C.L. Yiin, S.S. Lam, Progress in thermochemical co-processing of biomass and sludge for sustainable energy, value-added products and circular economy, Bioresour. Technol. 380 (2023), https://doi.org/10.1016/j.biortech.2023.129061.

[11] RED III - Renewable Energy Directive.

[12] S. Papari, K. Hawboldt, A review on the pyrolysis of woody biomass to bio-oil: Focuson kinetic models, Renew. Sustain. Energy Rev. 52 (2015) 1580–1595, https://doi.org/10.1016/j.rser.2015.07.191.

[13] J.S. Kim, Y.Y. Lee, T.H. Kim, A review on alkaline pretreatment technology for bioconversion of lignocellulosic biomass, Bioresour. Technol. 199 (2016) 42–48, https://doi.org/10.1016/j.biortech.2015.08.085.

[14] X. Zhou, W. Li, R. Mabon, L.J. Broadbelt, A critical review on hemicellulose pyrolysis, Energ. Technol. 5 (2017) 52–79, https://doi.org/10.1002/ente.201600327.

[15] W.O.S. Doherty, P. Mousavioun, C.M. Fellows, Value-adding to cellulosic ethanol: Lignin polymers, Ind. Crop. Prod. 33 (2011) 259–276, https://doi.org/10.1016/j.indcrop.2010.10.022.

[16] K. Dussan, S. Dooley, R. Monaghan, Integrating compositional features in model compounds for a kinetic mechanism of hemicellulose pyrolysis, Chem. Eng. J. 328 (2017) 943–961, https://doi.org/10.1016/j.cej.2017.07.089.

[17] R.C. Pettersen, The Chemical Composition of Wood, in: The Chemistry of Solid Wood, 1984, pp. 57–126.

[18] J. Vogel, Unique aspects of the grass cell wall, Curr. Opin. Plant Biol. 11 (2008) 301–307, https://doi.org/10.1016/j.pbi.2008.03.002.

[19] P. Kostetskyy, L.J. Broadbelt, Progress in modeling of biomass fast pyrolysis: A review, Energy Fuel 34 (2020) 15195–15216, https://doi.org/10.1021/acs.energyfuels.0c02295.

[20] S. Hameed, A. Sharma, V. Pareek, H. Wu, Y. Yu, A review on biomass pyrolysis models: Kinetic, network and mechanistic models, Biomass Bioenergy 123 (2019) 104–122, https://doi.org/10.1016/j.biombioe.2019.02.008.

[21] E. Ranzi, P.E.A. Debiagi, A. Frassoldati, Mathematical Modeling of Fast Biomass Pyrolysis and Bio-Oil Formation, Note i: Kinetic Mechanism of Biomass Pyrolysis, ACS Sustain Chem Eng 5 (2017) 2867–2881, https://doi.org/10.1021/acssuschemeng.6b03096.

[22] T. Faravelli, A. Frassoldati, G. Migliavacca, E. Ranzi, Detailed kinetic modeling of the thermal degradation of lignins, Biomass Bioenergy 34 (2010) 290–301, https://doi.org/10.1016/j.biombioe.2009.10.018.

[23] E. Ranzi, A. Cuoci, T. Faravelli, A. Frassoldati, G. Migliavacca, S. Pierucci, S. Sommariva, Chemical kinetics of biomass pyrolysis, Energy Fuel 22 (2008) 4292–4300, https://doi.org/10.1021/ef800551t.
[24] T. Faravelli, A. Frassoldati, E. Barker Hemings, E. Ranzi, Multistep kinetic model of biomass pyrolysis, in: F. Battin-Leclerc, Simmie; John M.;, Blurock; Edward (Eds.), Cleaner Combustion. Green Energy and Technology, Springer, London, 2013: pp. 111–139. https://doi.org/10.1007/978-1-4471-5307-8_5.
[25] E. Ranzi, M. Corbetta, F. Manenti, S. Pierucci, Kinetic modeling of the thermal degradation and combustion of biomass, Chem. Eng. Sci. 110 (2014) 2–12, https://doi.org/10.1016/j.ces.2013.08.014.
[26] P. Debiagi, G. Gentile, A. Cuoci, A. Frassoldati, E. Ranzi, T. Faravelli, A predictive model of biochar formation and characterization, J. Anal. Appl. Pyrol. 134 (2018) 326–335, https://doi.org/10.1016/j.jaap.2018.06.022.
[27] R. Moriana, Y. Zhang, P. Mischnick, J. Li, M. Ek, Thermal degradation behavior and kinetic analysis of spruce glucomannan and its methylated derivatives, Carbohydr. Polym. 106 (2014) 60–70, https://doi.org/10.1016/j.carbpol.2014.01.086.
[28] S.D. Stefanidis, K.G. Kalogiannis, E.F. Iliopoulou, C.M. Michailof, P.A. Pilavachi, A. A. Lappas, A study of lignocellulosic biomass pyrolysis via the pyrolysis of cellulose, hemicellulose and lignin, J. Anal. Appl. Pyrol. 105 (2014) 143–150, https://doi.org/10.1016/j.jaap.2013.10.013.
[29] D.K. Shen, S. Gu, A.V. Bridgwater, Study on the pyrolytic behaviour of xylan-based hemicellulose using TG-FTIR and Py-GC-FTIR, J. Anal. Appl. Pyrol. 87 (2010) 199–206, https://doi.org/10.1016/j.jaap.2009.12.001.
[30] N. Worasuwannarak, T. Sonobe, W. Tanthapanichakoon, Pyrolysis behaviors of rice straw, rice husk, and corncob by TG-MS technique, J. Anal. Appl. Pyrol. 78 (2007) 265–271, https://doi.org/10.1016/j.jaap.2006.08.002.
[31] H. Yang, R. Yan, H. Chen, D.H. Lee, C. Zheng, Characteristics of hemicellulose, cellulose and lignin pyrolysis, Fuel 86 (2007) 1781–1788, https://doi.org/10.1016/j.fuel.2006.12.013.
[32] S. Wang, B. Ru, H. Lin, W. Sun, Pyrolysis behaviors of four O-acetyl-preserved hemicelluloses isolated from hardwoods and softwoods, Fuel 150 (2015) 243–251, https://doi.org/10.1016/j.fuel.2015.02.045.
[33] R. Bassilakis, R.M. Carangelo, M.A. Wójtowicz, TG-FTIR analysis of biomass pyrolysis, Fuel 80 (2001) 1765–1786.
[34] K. Werner, L. Pommer, M. Broström, Thermal decomposition of hemicelluloses, J. Anal. Appl. Pyrol. 110 (2014) 130–137, https://doi.org/10.1016/j.jaap.2014.08.013.
[35] W.H. Chen, P.C. Kuo, Torrefaction and co-torrefaction characterization of hemicellulose, cellulose and lignin as well as torrefaction of some basic constituents in biomass, Energy 36 (2011) 803–811, https://doi.org/10.1016/j.energy.2010.12.036.
[36] C. Branca, C. Di Blasi, C. Mango, I. Hrablay, Products and kinetics of glucomannan pyrolysis, Ind. Eng. Chem. Res. 52 (2013) 5030–5039, https://doi.org/10.1021/ie400155x.
[37] V. Piazza, R.B. da Silva Junior, A. Frassoldati, L. Lietti, S. Chiaberge, C. Gambaro, A. Siviero, T. Faravelli, A. Beretta, Detailed speciation of biomass pyrolysis products with a novel TGA-based methodology: the case-study of cellulose, J. Anal. Appl. Pyrolysis 178 (2024) 106413, https://doi.org/10.1016/j.jaap.2024.106413.
[38] P. Debiagi, V. Piazza, M. Papagni, A. Beretta, A. Frassoldati, T. Faravelli, Cellulose pyrolysis kinetic model: detailed description of volatile species, Proc. Combust. Inst., in press. https://doi.org/10.1016/j.proci.2024.105651.
[39] C.G. Visconti, E. Tronconi, L. Lietti, R. Zennaro, P. Forzatti, Development of a complete kinetic model for the Fischer-Tropsch synthesis over Co/Al2O3 catalysts, Chem. Eng. Sci. 62 (2007) 5338–5343, https://doi.org/10.1016/j.ces.2006.12.064.
[40] L. Majocchi, L. Lietti, A. Beretta, P. Forzattf, E. Micheli, L. Tagliabue, Synthesis of short chain alcohols over a Cs-promoted Cu/ZnO/Cr203 catalyst, Appl. Catal. A 166 (1998) 393–405.
[41] C.G. Visconti, M. Martinelli, L. Falbo, L. Fratalocchi, L. Lietti, CO2 hydrogenation to hydrocarbons over Co and Fe-based Fischer-Tropsch catalysts, Catal. Today 277 (2016) 161–170, https://doi.org/10.1016/j.cattod.2016.04.010.
[42] D. Lin, Z. Mao, X. Feng, X. Zhou, H. Yan, H. Zhu, Y. Liu, X. Chen, Y. Tuo, C. Peng, D. Chen, C. Yang, Kinetic insights into deoxygenation of vegetable oils to produce second-generation biodiesel, Fuel 333 (2023), https://doi.org/10.1016/j.fuel.2022.126416.
[43] W. Kuang, M. Lu, I. Yeboah, G. Qian, X. Duan, J. Yang, D. Chen, X. Zhou, A comprehensive kinetics study on non-isothermal pyrolysis of kerogen from Green River oil shale, Chem. Eng. J. 377 (2019), https://doi.org/10.1016/j.cej.2018.10.212.
[44] A. Cuoci, A. Frassoldati, T. Faravelli, E. Ranzi, OpenSMOKE++: An object-oriented framework for the numerical modeling of reactive systems with detailed kinetic mechanisms, Comput. Phys. Commun. 192 (2015) 237–264, https://doi.org/10.1016/j.cpc.2015.02.014.
[45] L. Burhenne, J. Messmer, T. Aicher, M.P. Laborie, The effect of the biomass components lignin, cellulose and hemicellulose on TGA and fixed bed pyrolysis, J. Anal. Appl. Pyrol. 101 (2013) 177–184, https://doi.org/10.1016/j.jaap.2013.01.012.
[46] A.H. Hubble, J.L. Goldfarb, Synergistic effects of biomass building blocks on pyrolysis gas and bio-oil formation, J. Anal. Appl. Pyrol. 156 (2021), https://doi.org/10.1016/j.jaap.2021.105100.
[47] C. Quan, N. Gao, Q. Song, Pyrolysis of biomass components in a TGA and a fixed-bed reactor: Thermochemical behaviors, kinetics, and product characterization, J. Anal. Appl. Pyrol. 121 (2016) 84–92, https://doi.org/10.1016/j.jaap.2016.07.005.
[48] J. Yu, N. Paterson, J. Blamey, M. Millan, Cellulose, xylan and lignin interactions during pyrolysis of lignocellulosic biomass, Fuel 191 (2017) 140–149, https://doi.org/10.1016/j.fuel.2016.11.057.
[49] F.X. Collard, J. Blin, A review on pyrolysis of biomass constituents: Mechanisms and composition of the products obtained from the conversion of cellulose, hemicelluloses and lignin, Renew. Sustain. Energy Rev. 38 (2014) 594–608, https://doi.org/10.1016/j.rser.2014.06.013.
[50] H. Zhou, Y. Long, A. Meng, S. Chen, Q. Li, Y. Zhang, A novel method for kinetics analysis of pyrolysis of hemicellulose, cellulose, and lignin in TGA and macro-TGA, RSC Adv. 5 (2015) 26509–26516, https://doi.org/10.1039/c5ra02715b.
[51] S. Wang, B. Ru, H. Lin, Z. Luo, Degradation mechanism of monosaccharides and xylan under pyrolytic conditions with theoretic modeling on the energy profiles, Bioresour. Technol. 143 (2013) 378–383, https://doi.org/10.1016/j.biortech.2013.06.026.
[52] X. Zhou, W. Li, R. Mabon, L.J. Broadbelt, A mechanistic model of fast pyrolysis of hemicellulose, Energy, Environ. Sci. 11 (2018) 1240–1260, https://doi.org/10.1039/c7ee03208k.
[53] G. Lv, S. Wu, Analytical pyrolysis studies of corn stalk and its three main components by TG-MS and Py-GC/MS, J. Anal. Appl. Pyrol. 97 (2012) 11–18, https://doi.org/10.1016/j.jaap.2012.04.010.
[54] T. Hosoya, H. Kawamoto, S. Saka, Pyrolysis behaviors of wood and its constituent polymers at gasification temperature, J. Anal. Appl. Pyrol. 78 (2007) 328–336, https://doi.org/10.1016/j.jaap.2006.08.008.